Thin Solid Films 589 (2015) 356–363

Contents lists available at ScienceDirect

Thin Solid Films

journal homepage: www.elsevier.com/locate/tsf

Comparison of mechanical and corrosion properties of graphene monolayer on Ti–Al–V and nanometric Nb_2O_5 layer on Ti–Al–V alloy for dental implants applications

M. Kalisz [a,*], M. Grobelny [a], M. Mazur [b], M. Zdrojek [c], D. Wojcieszak [b], M. Świniarski [c], J. Judek [c], D. Kaczmarek [b]

[a] Motor Transport Institute, Jagiellońska 80, 03-301 Warsaw, Poland
[b] Wroclaw University of Technology, Faculty of Microsystem Electronics and Photonics, Janiszewskiego 11/17, 50-372 Wroclaw, Poland
[c] Faculty of Physics, Warsaw University of Technology, Koszykowa 75, 00-662 Warsaw, Poland

ARTICLE INFO

Article history:
Received 25 November 2014
Received in revised form 17 March 2015
Accepted 24 May 2015
Available online 28 May 2015

Keywords:
Magnetron sputtering
Graphene monolayer
Nb_2O_5 thin film
Corrosion protection
Mechanical properties

ABSTRACT

In this paper the comparative studies on structural, mechanical and corrosion properties of Nb_2O_5/Ti–Al–V and graphene/Ti–Al–V alloy systems have been investigated. We show that the hardness of pure niobium pentoxide was ca. 8.64 GPa and graphene deposited on titanium alloy surface was equal 5.63 GPa. However, the graphene monolayer has no effect on surface hardness of titanium alloy and can be easily removed from the surface. On the other hand, the sample with graphene coating has much better corrosion resistance.
Our results suggest, that the use of combined layers of niobium pentoxide and graphene, in the hybrid multilayer system can greatly improve the mechanical and corrosion properties of the titanium alloy surface. Such hybrid system can be used in the future, as protection coating for Ti alloy, in biomedical application and in other applications, where Ti alloys work in an aggressive corrosive environment and in engineering applications where friction is involved.

1. Introduction

Many metallic materials, e.g. stainless steel or alloys based on Co–Cr or Ti are commonly used in biomedical applications [1–5]. Such materials fulfill the requirement of biomaterials, but according to some works [1,6] they also exhibit many disadvantages; e.g. mismatch between the material's and bone's elasticity, and the toxicity connected with the release of corrosive products. The wide application of titanium and its alloys in various fields of biomedicine is due to their excellent mechanical properties, good corrosion resistance in biological fluids and biocompatibility [7]. The excellent corrosion resistance of titanium in various test saliva solutions and other physiological media is due to the formation of protective oxide-TiO_2 layer on its surface [8]. Recently, we have observed an increased use of dental gels, toothpastes and rinses containing fluoride for dental prevention applications [9–11]. Fluoride-containing specimens have a high fluoride concentration (10,000 ppm) and a pH range between 3.2 and 7.2. Fluorides are inimical to all reactive metals such as titanium, especially in acidic media, causing corrosion due to destruction of their passivity (TiO_2 films) and loss of mechanical properties [12].Consequently this leads to the significant surface alteration and discoloration of Ti–Al–V alloy implants and prostheses. Ti ion release from Ti specimens was found to increase in the presence of fluoride with low pH, further accelerating this effect [13].

The average corrosion resistance of titanium alloys in specific conditions (i.e. solutions with a low pH and a high concentration of fluoride ions) is not the only problem. Titanium and its alloys are characterized by poor wear resistance and low tribo-corrosion performance [14,15]. The toxic products of corrosion process (taking place on a titanium alloy surface in specific environments) and the products released from it as a result of abrasion during the operation of an implant, can lead to inflammatory or allergic reactions and metalosis [16]. All these lead to the necessity of implant removal [20,21].

To overcome this problem it is necessary to further enlarge the implant surface. Numerous surface modifications of titanium alloy implants have been performed to improve their corrosion resistance, especially in specimens with a high fluoride concentration and low pH. These methods include burnishing and surface micro-shot peening and thermo-chemical treatment, in particular based on the physical vapor deposition (PVD) and chemical vapor deposition (CVD) methods [14,15,17].

One way of doing this, is to produce an oxide-based coating on the titanium alloy surface. This leads to the metal's insulation from environmental hazards by the continuous, durable and, at the same time, elastic oxide film [18].

One of materials that can be applied in this area is niobium oxide. Nb_2O_5 (niobia) exhibits high corrosion and wear resistance and it is a

* Corresponding author at: Motor Transport Institute, Center for Material Testing, Jagiellońska 80, Str. Warsaw, Poland. Tel.: +48 22 43 85 537.
E-mail address: malgorzata.kalisz@its.waw.pl (M. Kalisz).

http://dx.doi.org/10.1016/j.tsf.2015.05.059
0040-6090/

Table 1
Composition of Ti_6Al_4V titanium alloy.

Components, wt.%						
C	Fe	N	O	Al	V	Ti
0.08	0.25	0.05	0.20	5.50–6.75	3.5–4.5	bal

very stable material. Nb_2O_5 has been investigated as a possible candidate for corrosion barrier coatings [21–23]. As it was shown by Eisenbarth et al. [24,25] or Ochsenbein et al. [26] niobium oxide exhibits a good biocompatibility, thus it could be effectively used in biological applications. According to Ramirez et al. [27] Nb_2O_5 coatings prepared by magnetron sputtering could improve the performance of stainless steel dental implants. This happens because their surface hardness, corrosion resistance and biological response are enhanced. Moreover, it was found that there is a general relationship between deposition conditions and physicochemical properties of Nb_2O_5 thin films, but a lack of reports on the biocompatibility of these films is notable [18,28–30]. There has been some previous evidences that niobium oxide films, produced by the sol–gel method, exhibit good biological compatibility [19, 24–33] and good apatite-inducing ability by immersion in simulated body fluids (SBF) solution [31]. Other works show that, anodized niobium-based oxide coatings exhibit bioactivity in a variety of solutions including calcium-phosphorous solution [32], simulated and human salivas [33] and simulated blood fluid [34,35].

Another way to improve titanium alloys surface properties can be deposition of ultra thin graphene monolayer. Graphene is one of the most inspiring and promising materials studied in recent years. Studies have shown that a single graphene layer considerably increases the corrosion resistance of such systems as copper/graphene [36] and nickel/graphene [37,38] and protects the surfaces of those metals from oxidation [39].

The purpose of this manuscript is to show that graphene monolayer can be used as a layer for protection of titanium alloy surface against corrosion process. In this work, corrosion and mechanical properties of graphene/Ti–Al–V alloy system have been investigated and compared with pure titanium alloy and Nb_2O_5/Ti–Al–V alloy system.

2. Materials and methods

2.1. Specimen preparation

For the purpose of the experiment, three sets of titanium alloys (Ti_6Al_4V) ASTM Grade 5, UNS R56400 (Table 1) samples were prepared in the same manner. Before technological processes, the Ti alloy surfaces were polished using a grinding and polishing Stuers RotoPol 21apparatus. The sample surface was polished to a "mirror image". In the next stage, samples were cleaned in an acetone solution.

2.2. Thin films preparation

2.2.1. Graphene/Ti–Al–V system preparation

The graphene monolayers were grown on 18-μm thick copper foil using chemical vapor deposition (CVD) technique (using home-made CVD set based on Blue M Tube Furnace with 1-inch diameter reactor tube).

Graphene was transferred on titanium alloy substrate using "PMMA-mediated" method [39]. First, PMMA (495 K, about 100 nm thick) was spin-coated on top of the synthesized graphene on copper substrate and dried for 24 h at room temperature. Next the graphene from bottom of Cu substrate was etched by reactive ion etching method in oxygen plasma (PlasmaLab 80 +, Oxford Instruments). After that, the exposed Cu foil was dissolved in an aqueous etchant of iron (III) nitrate for several hours. When the copper is dissolved the graphene sample was cleaned in deionized water. Next, ion particles have been removed using hydrochloric acid solution and hydrogen peroxide as catalyst dissolved in water [39]. After all cleaning steps, PMMA/graphene layer was transferred on a titanium alloy substrate and annealed in order to evaporate water and increase adhesion between graphene and the surface. In the last step the PMMA layer was removed.

2.2.2. Niobium oxide/Ti–Al–V system preparation

Thin film was prepared by magnetron sputtering method. An innovative multi-target apparatus was used for the deposition process [40]. This system allows deposition of composite coatings on up to four targets. In this work, metallic niobium target was sputtered in a pure oxygen atmosphere and the working pressure during the sputtering was equal to ca. $3 \cdot 10^{-3}$ mbar. The thickness of the deposited thin film was measured by Taylor Hobson Talysurf CCI Lite optical profilometer.

2.3. Analysis of surface characteristics

The quality and a number of transferred layers of graphene were evaluated by Raman spectroscopy (InVia Renishaw Spectrometer, 514 nm laser line, standard and streamline mode). All Raman spectra were collected at room temperature using 1 mW of laser power (on the sample).

Raman spectroscopy is a nondestructive and fast method for studying various carbon materials. In case of graphene, Raman spectra gives information about number of layers [41,42], material quality and defects [42,43]. Typical Raman spectra consist of 3 main modes: D mode (~1350 cm^{-1}), G mode (~1580 cm^{-1}) and 2D mode (~2700 cm^{-1}). Monolayer graphene sheet is easily identified by Raman study simply by looking at the G/2D relative intensity ratio (usually about 0.2), also taking into account the shape of those peaks [41,42]. The quality and defectiveness of graphene sheet can be verified by appearance of D mode peak, usually measured by looking at the relative intensity ratio ID/IG of peaks D and G [42,44].

The elemental composition and the surface morphology of the nioba coating and graphene monolayer were investigated with the aid of FESEM FEI Nova NanoSEM 230 scanning electron microscope (SEM). The SEM images were obtained using a low voltage high contrast vCD detector, which is effective for low voltage (<3 kV) backscattered electron imaging.

To determine the surface topography properties, atomic force microscopy (AFM) measurements were made by a UHV VT AFM/STM Omicron (Oxford Instruments, Germany) microscope operating in ultra-high vacuum conditions in contact mode. In the case of prepared coating, the root mean square (RMS) surface roughness was

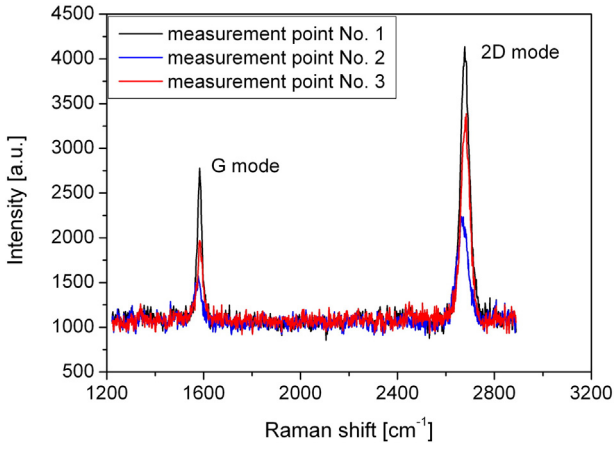

Fig. 1. Comparison of Raman spectra obtained for three different measurement points on the sample Ti–Al–V covered by graphene layer.

Table 2
Parameters of the spectrum obtained from Raman spectroscopy, in three different measurement points on the sample covered by single layer of graphene.

Point No.	G mode position [cm^{-1}]	FWHM G [cm^{-1}]	G mode intensity	2D mode position [cm^{-1}]	FWHM 2D	2D mode intensity	IG/I2D
1	1583	20	54,311	2678	40	200,721	0.27
2	1576	34	26,270	2668	49	93,277	0.28
3	1585	24	32,920	2679	39	144,561	0.23

calculated from five different AFM images and the standard deviation of this parameter was determined.

X-ray photoelectron spectroscopy (XPS) studies were performed to determine the chemical states of niobium and oxygen at the surface of thin film with the aid of Specs Phoibos 100 MCD-5 (5 single channel electron multiplier) hemispherical analyzer (SPECS Surface Nanoanalysis GmbH) using the Specs XR-50 X-ray source with Mg Kα (1253.6 eV) beam. The results of the measurements were then analyzed with the aid of CasaXPS software. The Nb4d spectra were calibrated with respect to the binding energy of the adventitious C1s peak at 284.8 eV.

2.4. Mechanical characterization

The hardness measurements of the obtained coatings were performed by the nanoindenter manufactured by CSM Instruments equipped with a diamond Vickers indenter. The hardness was calculated using the method proposed by Oliver and Pharr [45]. Each data point represents an average of five indentations. A number of measurements were carried out for various depths of nanoindentation (from 80 nm to 700 nm). In order to measure the "film-only" properties and minimize the impact of the substrate, a method of nanoindentation measurements approximation was implemented [46]. The measured hardness of the thin film deposited on a substrate can be expressed as a power-low function of the substrate and the thin film hardness, the depth of nanoindentation and the thickness of thin film [46]:

$$H = H_S\left(\frac{H_f}{H_S}\right)^M \tag{1}$$

where: H_s – hardness of substrate, H_f – hardness of thin film, and M – dimensionless spatial function defined by [47]:

$$M = \frac{1}{1 + A\left(\frac{h}{d}\right)^B} \tag{2}$$

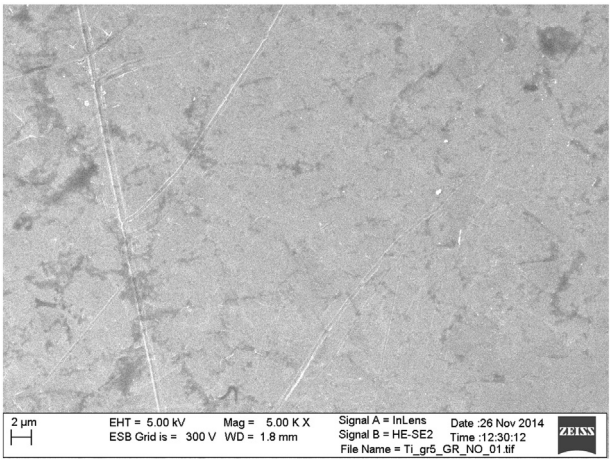

Fig. 2. SEM images of the titanium specimens with graphene layer.

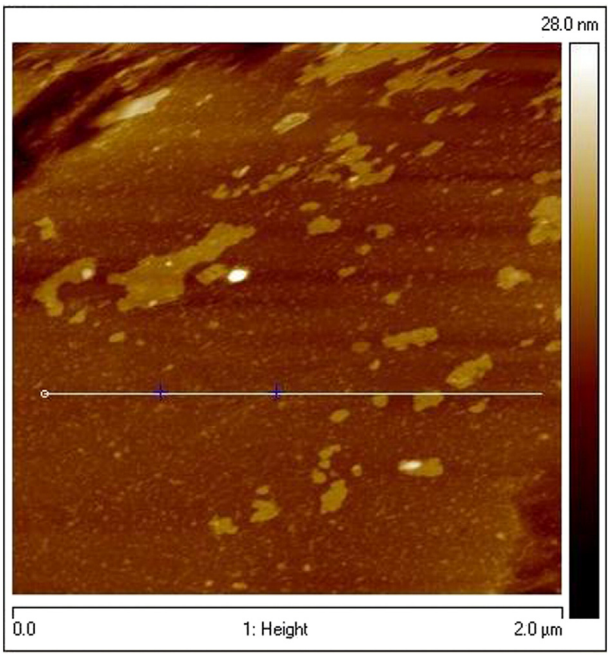

Fig. 3. Results of the measurement of graphene monolayer by AFM.

where A, B – adjustable coefficients, h – maximum intender displacement, and d – thickness of thin film.

Eq. (1) must satisfy essential boundary conditions: when the indentation depth approaches zero (small indentation displacements), the measured hardness tends to the thin film hardness, whereas when the indentation depth approaches the thin film thickness, measured hardness tends to the value of substrate hardness.

The abrasion resistance of the Nb_2O_5 thin film was investigated using a Summers Optical's Lens Coating Hardness Test Kit (EMS Acquisition Corp., USA). On the basis of the experiments, scratch resistance was evaluated. For the purpose of abrasion resistance examination, a steel wool test was carried out which consisted of rubbing the surface of the prepared coating with 0 grade steel wool pad using an applied load of 0.5 N. The steel wool pad was pressed on the surface of the coating with the given force and was moved across the surface of thin film for 75 cycles. The abrasion resistance test was performed for the transparent metal oxide coatings according to the well-acknowledged standard [48] and literature reports (e.g. [49]). The surface was examined for scratch resistance by an optical microscope and a profilometer. Three-dimensional images of the surface of the investigated coating, before and after the scratch tests, were obtained with the aid of a TalySurf

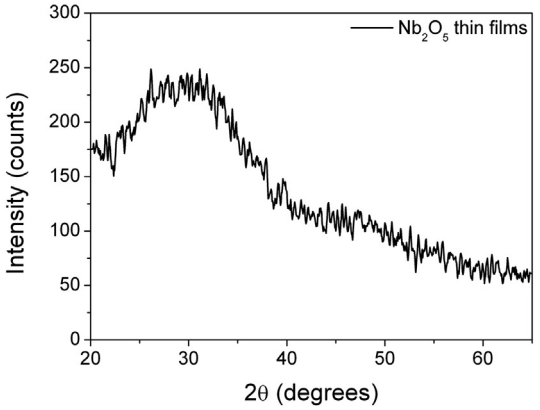

Fig. 4. Results of the measurements of Nb_2O_5 thin films by XRD.

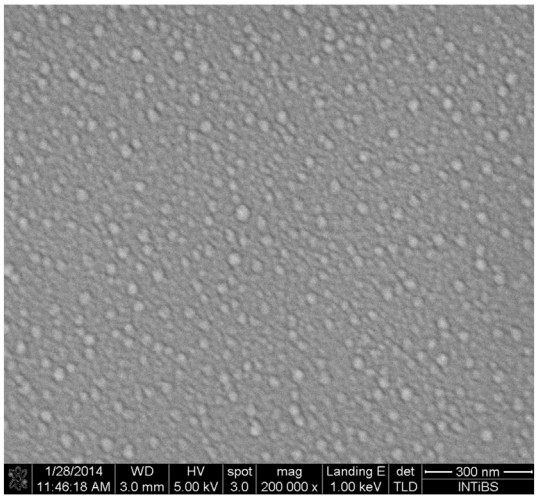

Fig. 5. SEM images of as-deposited Nb_2O_5 thin film.

CCI Lite Taylor Hobson profilometer. The depth of scratches and change of roughness were evaluated.

2.5. Electrochemical measurements

Electrochemical measurements were carried out in 0.5 M/l NaCl, 2 g/l KF, pH 2 adjusted by concentrated hydrochloric acid. The solution (0.5 M NaCl, pH 2 2 g/l KF) in which the electrochemical measurements were conducted is characterized by a high corrosivity compared to titanium alloys [50–52]. It is a more aggressive environment than that of typical electrolytes for corrosion tests (e.g. artificial saliva, SBF). The voltammetric measurements (polarization curves) were carried out at a scan rate of 1 mV/s within the range of −150 mV to 1000 mV versus open circuit potentials, and polarization curves corresponding to every examined material were recorded. Prior to each polarization experiment, the samples were immersed in the electrolyte for 1 h while monitoring open circuit potential to establish steady state conditions. Each electrochemical measurements for the same material, was performed for three times. In the paper, the most representative result was used. However, the differences between the successive values of the open circuit potential (for the same material) did not exceed 50 mV. A three-electrode cell arrangement was applied using the Ag/AgCl electrode with a Luggin capillary as reference electrode and a platinum wire as the auxiliary electrode (counter electrode). The measurements were carried out by means of an Autolab EcoChemie System of the AUTOLAB PGSTAT 302N type equipped with GPESv. 4.9 software in aerated solutions in room temperature. The values of corrosion current densities (i_{corr}) were obtained from the polarization curves by extrapolation of the cathodic and anodic branch of the polarization curves to the corrosion potential [53].

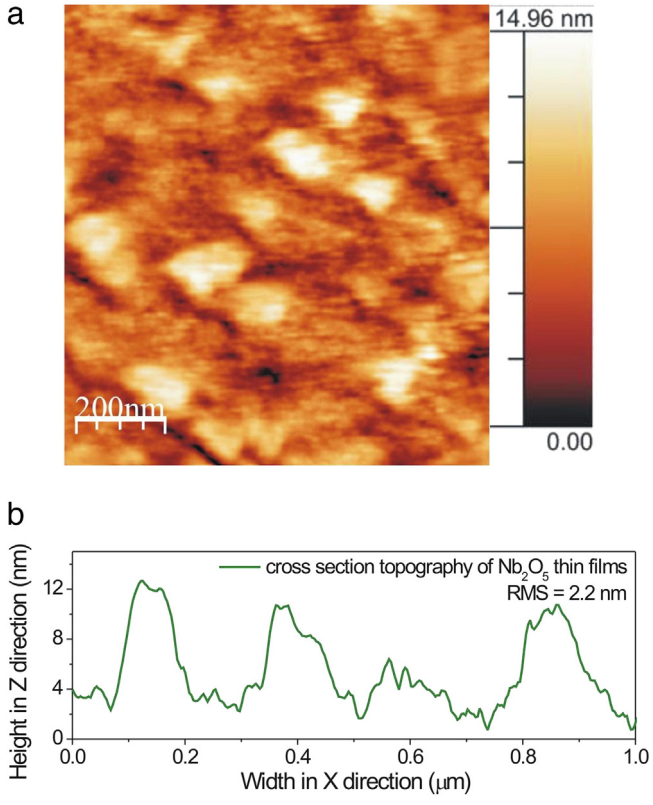

Fig. 6. AFM images (a) and cross-section topography (b) of deposited thin film.

3. Results and discussion

3.1. Structural characterization graphene/Ti–Al–V system and niobium pentoxide/Ti–Al–V system

3.1.1. Raman characterization of graphene/Ti–Al–V system

Fig. 1 shows the comparison of graphene/Ti–Al–V Raman spectra collected in three different places on the sample. In Table 2 there are presented all important parameters of the spectrum i.e. position of the peaks G, D and 2D and their intensities, which indicate the quality of the graphene layer. The Raman measurements have been repeated

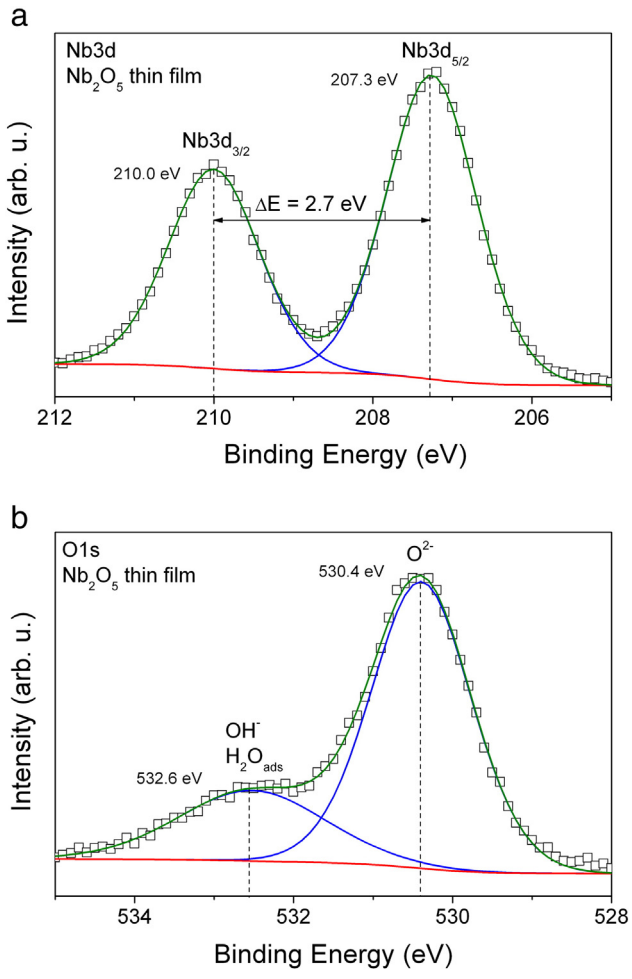

Fig. 7. XPS spectra of deposited Nb_2O_5 thin film.

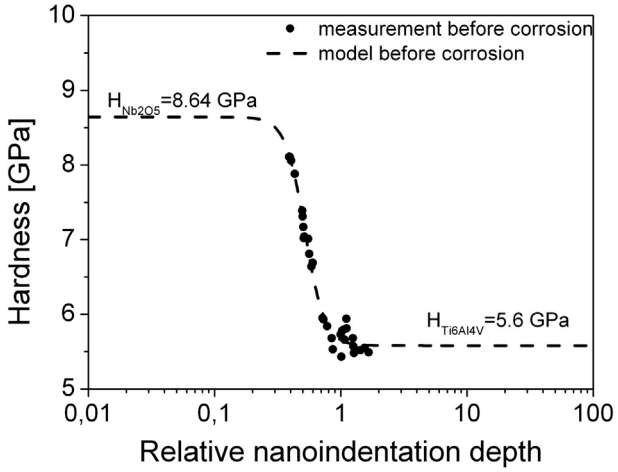

Fig. 8. Results of investigation of Nb_2O_5 hardness.

several times in many places on the samples (only representative data shown in Fig. 1), confirming the uniformity of the quality of the deposited graphene monolayer.

The large G/2D ratios ~0.2, obtained for all measurement points indicate that on the titanium alloy surface, there exists a single layer of graphene [41,42]. Small D peak (~1350 cm^{-1}) intensity indicates that the obtained on titanium alloy surface single layer of graphene has no defects, which proves that it has not been damaged during transfer process on the Ti–Al–V surface.

3.1.2. Structural characterization of graphene/Ti–Al–V system

In Fig. 2, SEM image of the surface of the Ti–Al–V/graphene system is shown. The deposited graphene coating was crack-free, no discontinuous coating was observed and the surface morphology was homogeneous.

The two-dimensional AFM image is shown in Fig. 3. As in the case of SEM measurements (as shown in Fig. 2), the AFM measurements show no cracks and no discontinuities for the graphene monolayer deposited on titanium alloy surface. The surface of graphene was flat and homogenous. The titanium alloy regions under the graphene flakes were pristine and shiny, which indicates that these regions were not oxidized.

3.1.3. Structural characterization of niobium pentoxide/Ti–Al–V system

The thickness of the deposited thin film was equal to 210 nm. The investigated film deposited by reactive magnetron sputtering in pure oxygen plasma was amorphous since no characteristic peaks were observed in the XRD pattern (Fig. 4). The amorphous structure of the deposited thin film may be a result of the low temperature of the sputtering process and the fact that substrate was not additionally heated during deposition.

In Fig. 5 SEM image of the surface of the investigated thin film is shown. The deposited Nb_2O_5 thin film was crack-free, exhibited good adherence to the substrate, no discontinuities of the thin film were observed and the surface morphology was homogeneous. The particles were visible in the image of a nioba thin film and had uniform shape.

The AFM measurements were performed in order to extend the information regarding the surface topography of the Nb_2O_5 coating. The two-dimensional AFM image is shown in Fig. 6a. The surface of Nb_2O_5 was crack-free, densely packed and composed of visible grains, whose height was ca. 6–10 nm. It was confirmed by the cross-section topography of the surface that is also presented in Fig. 6b.

The height distribution of grains is symmetric, which proves its homogenous surface and the calculated root mean square (RMS) was found to be equal to 2.2 nm ± 0.5 nm.

The XPS measurements were performed to determine the chemical states of the niobium and oxygen on the surface of the prepared thin film. In Fig. 7 the Nb3d and O1s core level spectra are presented for as-deposited Nb_2O_5 coating. The position of the Nb3d doublet and the separation energy width equal to 2.7 eV between the peak of $Nb3d_{5/2}$ and $Nb3d_{3/2}$ indicates on the Nb^{5+} oxidation state, what is an evidence of the formation of Nb_2O_5 oxides [54,55]. The representative O1s XPS spectra for the deposited thin film were deconvoluted into two components related to the lattice oxygen of nioba oxides at ca. 530.2–530.4 eV and oxygen bonded on the surface at ca. 532.1–532.6 eV [55]. The lower peak located at higher binding energy is attributed to adsorbed water molecules (H_2O_{ads}) and hydroxyl radicals (OH^-). The results obtained for the O1s oxidation state revealed that the summarized level of the oxygen related to the H_2O_{ads} and OH^- is equal to ca. 24.8% of the oxygen bonds overall occurring at the surface of the investigated thin film.

3.2. Mechanical properties

The hardness values of the titanium alloy, prepared niobium pentoxide layer and graphene monolayer were measured by nanoindentation and determined by an approximation method. For the pure titanium alloy and titanium alloy covered by graphene monolayer, hardness values were measured at a constant depth equal to 80 nm. It is the smallest depth, for which the correct results have been obtained. The obtained values for the investigated films were based on the average of the five measured points. Additionally, the RMS error was calculated.

The determined hardness was equal to (5.64 ± 0.21) GPa for the uncoated titanium alloy (5.62 ± 0.22), GPa for titanium alloy covered by graphene monolayer and 8.64 GPa for Nb_2O_5 layer (Fig. 8). As compared to the results presented in the literature reports, the hardness of the

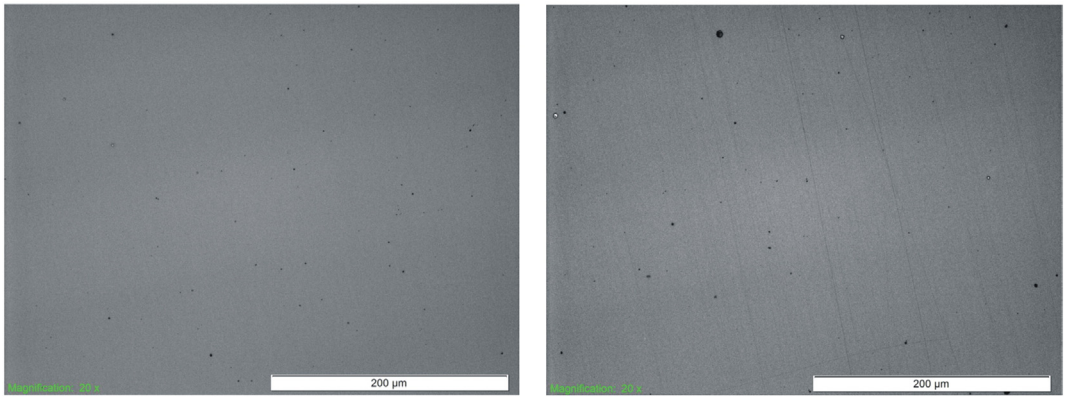

Fig. 9. Optical microscopy images of as-deposited Nb_2O_5 coating before (left side) and after (right side) performing scratch tests.

investigated Nb_2O_5 thin film is higher by ca. 50% [55], 53% [56] and 46% [57]. RMS error for hardness approximation was equal to 0.12 GPa for pure Nb_2O_5.

Graphene layer deposited on titanium alloy surface is practically not seen by nanoindenter during measurements. Therefore, the measurement did not reveal changes of titanium alloy surface hardness after graphene deposition (compared to pure titanium alloy), and was equal to 5.62 GPa.

The obtained result showed that only a niobium pentoxide layer deposited on titanium alloy surface can be considered as a coating that improves the surface hardness of the Ti_6Al_4V alloy.

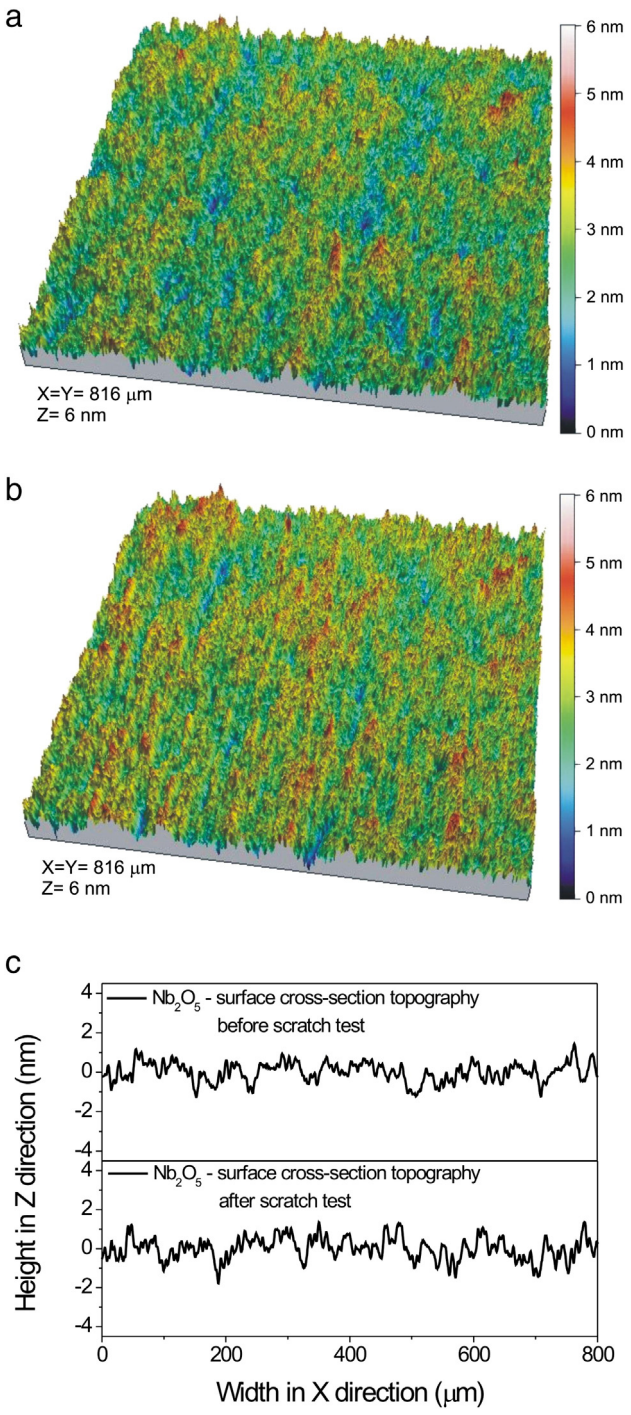

Fig. 10. Optical profilometry investigation results before (a), after (b) scratch tests and cross-section topographies (c) of Nb_2O_5 thin film.

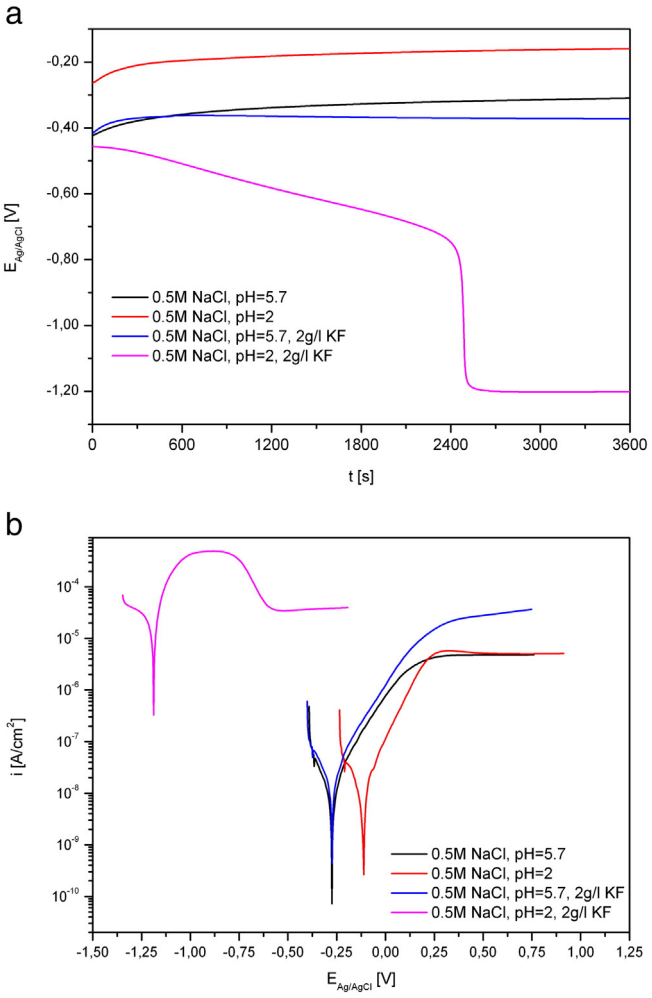

Fig. 11. Open circuit potentials (a) and polarization curves (b) of titanium alloy in various chloride solutions.

The tribological properties of the prepared thin film were determined using steel wool test with the applied load of 0.5 N. The optical microscopy images (Fig. 9) of pure nioba showed that no significant scratches were observed on the surface of the thin film.

The depth of scratches was evaluated with the aid of a Taylor Hobson profilometer and the results of these investigations are shown in Fig. 10a–c.

As in the case of the optical microscope measurements (as shown in Fig. 9), during the profilometry investigation, no significant scratches were found for nioba thin film. The cross-section topographies of the investigated thin film after scratch tests are also presented in Fig. 10c.

The mean arithmetical surface height measured with the aid of the optical profilometer changed from 0.53 nm for as-deposited undoped nioba to 0.55 nm after performing scratch tests. Therefore, the prepared thin film may be considered scratch resistant coating.

Table 3
Influence of the electrolyte composition on the electrochemical parameters of the Ti_6Al_4V titanium alloy obtained from polarization curves.

Electrolyte solution	i_{corr} [nA/cm^2]	E_{corr} [V]
0.5 M NaCl; pH 5.7	12.7	−0.275
0.5 M NaCl; pH 2	15.9	−0.113
0.5 M NaCl; pH 5.7; 2 g/l KF	30.6	−0.275
0.5 M NaCl; pH 2; 2 g/l KF	60500.0	−1.188

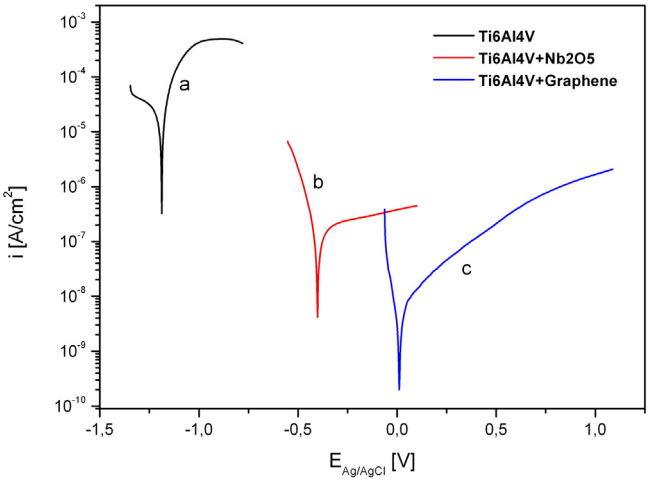

Fig. 12. Polarization curves of titanium alloy with deposited Nb_2O_5 thin film and graphene monolayer in 0.5 M/l NaCl, 2 g/l, pH 2 electrolyte solution.

The scratch resistance properties and the hardness properties of Nb_2O_5 thin film deposited on titanium alloy surface would be beneficial for the long-term performance of implants. Such coating would prevent the deterioration of the surface of biomaterials caused by various environmental hazards.

In the case of graphene layer, the obtained results showed that graphene monolayer deposited on titanium alloy surface was not resistant to abrasion. It was very easy to scratch and remove it from the titanium alloy surface, without the use of tools.

3.3. Corrosion properties

To show the effect of the solution type and pH on the corrosion properties of titanium alloys, four kinds of solutions were used and compared: neutral sodium chloride (0.5 M NaCl, pH 5.7), neutral sodium chloride with F^- (0.5 M NaCl, pH 5.7, 2 g/l KF), acid sodium chloride solution (0.5 M NaCl, pH 2) and acid sodium chloride solution with the addition of fluoride ions (0.5 M NaCl, 2 g/l KF, pH 2). Fig. 11 illustrates the effect of electrolyte type on the course of open circuit potentials and on the polarization curves for Ti_6Al_4V titanium alloy. The results of measurements of electrochemical parameters of the samples obtained from these curves are collected in Table 3.

The obtained results present a clear evidence that corrosion properties of titanium alloy strongly depend on composition of the used electrolyte. The lower rate of corrosion processes expressed by the lower corrosion current i_{corr}, was observed in the neutral solution. In this kind of solution the titanium oxides may appear on the surface of the metal. This passivation layer isolates the surface, resulting in a decrease of corrosion current.

The use of acid solution containing fluoride ions as the electrolyte solution leads to a significant increase in the rate of corrosion processes, and expressed an increase of corrosion current from 0.01 μA/cm^2 in neutral solution to 60,500 nA/cm^2.

Table 4
Electrochemical parameters of the samples obtained from polarization curves in 0.5 M/l NaCl, 2 g/l KF, pH 2 electrolyte solution.

Sample	i_{corr} [μA/cm^2]	E_{corr} [V]
Ti_6Al_4V	60.50	−1.188
Ti_6Al_4V/Nb_2O_5	0.24	−0.401
Ti_6Al_4V/Graphene	0.01	0.011

The change of corrosion potential depending on a type of electrolyte was also observed. In neutral NaCl, E_{corr} was −0.275 V, while for the acid solution with F^- ions $E_{corr} = -1.188$ V. In 0.5 M/l NaCl, 2 g/l KF, pH 2 solution the corrosion potential was more negative, so closer to the potential of pure metal titanium.

Fig. 12 presents polarization curves of titanium alloy and titanium alloy with deposited Nb_2O_5 and graphene in 0.5 M/l NaCl, 2 g/l KF, pH 2 electrolyte solution. The thin films on the surface of titanium alloy caused a significant decrease in the value of corrosion current densities (i_{corr}) (Table 4). However, the smallest corrosion current density, i.e. the better corrosion properties, was obtained for sample covered by monolayer of graphene. The presence of thin films on the surface of titanium alloy also resulted in changes in the value of corrosion potentials E_{corr} (Table 4). In this case, the biggest change of E_{corr} was observed for the samples with the monolayer of graphene. The shift of the corrosion potential in the noble direction decreases the electrochemical activity of the surface. This results in the improvement of corrosion resistance of the titanium alloy which is caused by the presence of the graphene monolayer.

4. Summary

Based on structural, mechanical and electrochemical measurements, the following conclusions can be drawn:

- The Nb_2O_5 thin film deposited by reactive magnetron sputtering is amorphous, crack-free, exhibits good adherence to the substrate and has homogeneous surface morphology.
- Deposition of pure nioba thin film on titanium alloy surface improves its surface hardness and corrosion properties. The hardness increases from 5.64 GPa (for titanium alloy) to 8.64 GPa (for Nb_2O_5 thin film). The corrosion current density significantly decreases from 60.50 μA/cm^2 (for titanium alloy) to 0.24 μA/cm^2 (for Nb_2O_5/Ti_6Al_4V alloy system). The Nb_2O_5 thin film is characterized by higher corrosion resistance.
- Graphene monolayer deposited on titanium alloy surface does not change surface mechanical properties of titanium alloy. However, there is considerable improvement to its corrosion properties in comparison with a nioba thin film (210 nm) in 0.5 M/l NaCl, 2 g/l KF, pH 2 electrolyte solution. The value of the corrosion current densities for graphene/Ti–Al–V alloy system was equal 0.01 μA/cm^2 while for nioba/Ti–Al–V alloy system – 0.24 μA/cm^2. Graphene monolayer caused also the shift of corrosion potential towards noble direction.

The obtained results have shown that niobium pentoxide layer and graphene monolayer deposited on titanium alloy surfaces, can be considered as a barrier coatings for the Ti_6Al_4V alloy. They protect its surface against corrosion processes, which take place on pure titanium alloy surface in very aggressive environments. Instead, only the Nb_2O_5 layer improved titanium alloy mechanical properties (i.e. surface hardness and wear resistance) and protects the titanium surface from the release of toxic products of corrosion and the abrasion process to the environment, which can cause allergies and metalosis.

It appears reasonable to perform combination of two types of coatings with hybrid system, which improves mechanical and corrosion properties of the titanium alloy surface. The proposed hybrid system is composed of mechanically resistive niobium pentoxide layer and graphene monolayer, which is characterized by very high corrosion resistance. But in this case, much more experimental work needs to be performed.

In the next step, the durability of corrosion and mechanical properties of hybrid systems during temporary exposure in corrosive environments (artificial saliva, SBF etc.) and also biocompatibility investigations will be performed.

Acknowledgments

This work was funded by the NCN in the years 2013–2016 as a research project number UMO-2012/07/B/ST8/03760.

This work was funded by the National Centre for Research and Development in the years 2013–2016 as research project number GRAF-TECH/NCBR/14/26/2013 (InGrafTi).

References

[1] P. Amaravathy, S. Sowndarya, S. Sathyanarayanan, N. Rajendran, Novel sol gel coating of Nb_2O_5 on magnesium alloy for biomedical applications, Surf. Coat. Technol. 244 (2014) 131.
[2] J. Wang, L. Wang, S. Guan, S. Zhu, C. Ren, S. Hou, Microstructure and corrosion properties of as sub-rapid solidification Mg–Zn–Y–Nd alloy in dynamic simulated body fluid for vascular stent application, J. Mater. Sci. Mater. Med. 21 (2010) 2001.
[3] Y. Luo, L. Yang, M. Tian, M. Tian, Application of biomedical-grade titnium alloys in trabecular bone and artificial joints, Biomater. Med. Tribol. (2013) 181.
[4] K. Narita, M. Niinomi, M. Nakai, Effects of micro- and nano-scale wave-like structures on fatigue strength of a beta-type titanium alloy developed as a biomaterial, J. Mech. Behav. Biomed. Mater. 29 (2014) 393.
[5] H. de Almeida, I.N. Bastos, I.D. Santos, A.J.B. Dutra, C.A. Nunes, S.B. Gabriel, Effects of micro- and nano-scale wave-like structures on fatigue strength of a beta-type titanium alloy developed as a biomaterial, J. Alloys Compd. 615 (2014) S666, http://dx.doi.org/10.1016/j.jallcom.2014.01.173.
[6] M. Geetha, A.K. Singh, R. Asokamani, A.K. Gogia, Ti based biomaterials, the ultimate choice for orthopaedic implants – A review, Proc. Math. Sci. 54 (2009) 397.
[7] K. Elagli, M. Traisnel, H.F. Hildebrand, Electrochemical behaviour of titanium and dental alloys in artificial saliva, Electrochim. Acta 38 (1993) 1764.
[8] A.M. Al-Mayouf, A.A. Al-Swayih, N.A. Al-Mobarak, Effect of potential on the corrosion behavior of a new titanium alloy for dental implant applications in fluoride media, Mater. Corros. 55 (2004) 88.
[9] P. Gilbert, J. Das, I. Foley, Biofilm Susceptibility to Antimicrobials, Adv. Dent. Res. 11 (1997) 160.
[10] O.G. Gold, H.V. Jordan, A selective medium for Streptococcus mutans, Arch. Oral Biol. 18 (1973) 1357.
[11] B.G. Bibby, The use of fluorine in the prevention of dental caries. I. Rationale and approach, J. Am. Dent. Assoc. 31 (1944) 228.
[12] C.P. Dillon, Phorgotten Phenomena: Behavior of Reactive Metals, Mater. Perform. 7 (1998) 69.
[13] R. Strietzel, A. Hosch, In vitro corrosion of titanium, Biomaterials 19 (1998) 1495.
[14] S. Thamizhmnaii, B. Bin Omar, S. Saparudin, S. Hasan, Surface roughness investigation and hardness by burnishing on titanium alloy, J. Achiev. Mater. Manuf. Eng. 28 (2) (2008) 139.
[15] K.-T. Rie, Th. Lampe, Thermochemical surface treatment of titanium and titanium alloy Ti_6Al_4V by low energy nitrogen ion bombardment, Mater Sci. Eng. 69 (2) (1985) 473.
[16] V.D. Mirjania, R.R. Arbutina, J.P. Šetrajaia, L.D. Dymbas, Physical properties of thin films on implant-materials, Prog. Nat. Sci. 118 (2010) 121.
[17] Y. Song, Z. Zhao, F. Lu, Experimental Study of the Influence of Shot Peening on the Microstructure and Properties of Surface Layer of a TC21 Titanium Alloy Titan, Alloy Atl. J. Mater. Sci. 1 (1) (2014) 17.
[18] X. Liua, P.K. Chub, Ch. Dinga, Surface modification of titanium, titanium alloys, and related materials for biomedical applications, Mater Sci. Eng. 47 (2004) 49.
[19] S. Anne Pauline, N. Rajendran, Biomimetic novel nanoporous niobium oxide coating for orthopaedic applications, Appl. Surf. Sci. 290 (2014) 448.
[20] J.H. Xie, R.L. Luan, Microstructural and electrochemical characterization of hydroxyapatite-coated Ti_6Al_4V alloy for medical implants, J. Mater. Res. 23 (2008) 768.
[21] J.-P. Masse, H. Szymanowski, O. Zabeida, A. Amassian, J.E. Klemberg-Sapieha, L. Martinu, Stability and effect of annealing on the optical properties of plasma-deposited Ta2O5 and Nb_2O_5 films, Thin Solid Film 515 (2006) 1674.
[22] D. Velten, E. Eisenbarth, N. Schanne, J. Breme, Biocompatible Nb_2O_5 thin films prepared by means of the sol–gel process, J. Mater. Sci. Mater. Med. 15 (2004) 457.
[23] J. Breme, R. Thull, J. Kirkpatrick, Metallic Biomaterial Interfaces, 1st ed. WILEYVCH Verlag GmbH & Co KGaA, Weinheim, 2008.
[24] E. Eisenbarth, D. Velten, M. Muller, R. Thull, J. Breme, Nanostructured niobium oxide coatings influence osteoblast adhesion, J. Biomed. Mater. Res. Part A 79A (2006) 166.
[25] E. Eisenbarth, D. Velten, J. Breme, Biomimetic implant coatings, Biomol. Eng. 24 (2007) 27.
[26] A. Ochsenbein, F. Chai, S. Winter, M. Traisnel, J. Breme, H.F. Hildebrand, Osteoblast responses to different oxide coatings produced by the sol–gel process on titanium substrates, Acta Biomater. 4 (2008) 1506.
[27] G. Ramirez, S.E. Rodil, H. Arzate, S. Muhl, J.J. Olaya, Niobium based coatings for dental implants, App. Surf. Sci. 257 (2001) 2555.
[28] S. Venkataraj, R. Drese, O. Kappertz, R. Jayavel, M. Wuttig, Characterization of Niobium Oxide Films Prepared by Reactive DC Magnetron Sputtering, Phys. Status Solidi A 188 (2001) 1047.
[29] F. Chai, A. Ochsenbein, M. Traisnel, R. Busch, J. Breme, H.F. Hildebrand, Improving endothelial cell adhesion and proliferation on titanium by sol–gel derived oxide coating, J. Biomed. Mater. Res. A 92 (2010) 754.
[30] C.A. Scotchford, M. Ball, M. Winkelmann, J. Voros, C. Csucs, D.M. Brunette, G. Danuser, M. Textor, Chemically patterned, metal-oxide-based surfaces produced by photolithographic techniques for studying protein- and cell-interactions. II: Protein adsorption and early cell interactions, Biomaterials 24 (2003) 1147.
[31] T. Miyazaki, Development of bioactive materials based on bone-bonding mechanism on metal oxides, J. Ceram. Soc. Jpn. 116 (2008) 260.
[32] R.L. Karlinsey, K. Yi, C.W. Duhn, Nucleation and growth of apatite by self-assembled polycrystalline bioceramics, Bioinspir. Biomim. 1 (2006) 12.
[33] R.L. Karlinsey, A.T. Hara, K. Yi, C.W. Duhn, Bioactivity of novel self-assembled crystalline Nb_2O_5 microstructures in simulated and human salivas, Biomed. Mater. 1 (2006) 16.
[34] R.L. Karlinsey, K. Yi, Self-assembly and bioactive response of a crystalline metal oxide in a simulated blood fluid, Mater. Med. 19 (2007) 1349.
[35] A. Mackey, R.L. Karlinsey, A. Chern, T.G. Chu, The growth kinetics and in vitro biocompatibility of Nb_2O_5 microcones, Inter J. Med. Eng. Inf. 2 (2010) 247.
[36] Ellie Teo, Yi Lih, Rubaiyi bt. Mat Zaid, Tan Ling Ling, Kwok Feng Chong, Facile Corrosion Protection Coating from Graphene, Inter. J. Chem. Eng. Appl. 3 (6) (2012) 3253.
[37] K. Jiang, J. Li, J. Liu, Electrochemical codeposition of graphene platelets and nickel for improved corrosion resistant properties, RSC Adv. 68 (2014) 36245.
[38] D. Prasai, Graphene: Corrosion-Inhibiting Coating, ACS Nano 6 (2012) 1102.
[39] X. Liang, B.A. Sperling, I. Calizo, G. Cheng, C.A. Hacker, Q. Zhang, Y. Obeng, K. Yan, H. Peng, Q. Li, X. Zhu, H. Yuan, A.R. Hight Walker, Z. Liu, L. Peng, C.A. Richter, Toward Clean and Crackless Transfer of Graphene, ACS Nano 5 (2011) 9144.
[40] D. Kaczmarek, J. Domaradzki, B. Adamiak, J. Dora, S. Maguda, *Polish patent application,* (2011), P396389.
[41] A. Gupta, G. Chen, P. Joshi, S. Tadigadapa, P.C. Eklund, Raman Scattering from High-Frequency Phonons in Supported n-Graphene Layer Films, Nano Lett. 6 (2006) 2667.
[42] A. Jorio, R. Saito, G. Dresselhaus, M.S. Dresselhaus, Raman Spectroscopy in Graphene Related Systems, Wiley-VCH, Weinheim, Germany, 2011.
[43] V. Singh, D. Joung, L. Zhai, S. Das, S.I. Khondaker, S. Seal, Graphene based materials: Past, present and future, Prog. Mater. Sci. 56 (2011) 1178.
[44] A.C. Ferrari, J.C. Meyer, V. Scardaci, C. Casiraghi, M. Lazzeri, F. Mauri, S. Piscanec, D. Jiang, K.S. Novoselov, S. Roth, A.K. Geim, Raman Spectrum of Graphene and Graphene Layers, Phys. Rev. Let. 97 (2006) 187401.
[45] W.C. Oliver, G.M. Pharr An, improved technique for determining hardness and elastic modulus using load and displacement, J. Mater. Res. 7 (1992) 1564.
[46] Y.-G. Jung, B.R. Lawn, M. Martyniuk, H. Huang, X.Z. Hu, Evaluation of elastic modulus and hardness of thin films by nanoindentation, J. Mater. Res. 19 (2004) 3076.
[47] B.V. Crist, Handbook of The Elements and Native Oxides, XPS International Inc, Iowa, USA, 1999.
[48] ISO/TC 172/SC 7/WG 3 N30 Standard, Spectacle lenses – Test method for abrasion resistance1998.
[49] R. Blacker, D. Bohling, M. Coda, M. Kolosey, Development of intrinsically conductive antireflection coatings for the ophthalmic industry, 43rd Annual Technical Conference Proceedings—Denver, April 15–20, Society of Vacuum Coaters 2000, p. 212.
[50] M. Nakagawa, T. Shiraishi Matsuya, M. Ohta, Effect of fluoride concentration and pH on corrosion behavior of titanium for dental use, J. Dent. Res. 78 (9) (1999) 1568.
[51] R.W. Schutz, D.E. Thomas, Corrosion of titanium and titanium alloys, 9th ed, Metals handbook, vol. 13, American Society for Metal (ASM) International, Metals Park, OH 1987, p. 669.
[52] L. Kinani, A. Chtaini, Corrosion Inhibition of Titanium in Artificial Saliva Containing Fluoride Leonardo, J. Sci. 12 (11) (2007) 33 (12(11)).
[53] F. Mansfeld, ASM Handbook, Electrochemical methods of corrosion testing, in: S.D. Cramer, B.S. Covino (Eds.), ASM Handbook, Corrosion Fundamentals, Testing and Protection USA, 13A, ASM International, USA 2003, p. 446.
[54] J. Moulder, W. Stickle, P. Sobol, K. Bomben, Handbook of X-ray Photoelectron Spectroscopy, Physical Electronics Inc, United States of America, 1995, ISBN 0-9648124-1-X.
[55] X. Zhou, Graphene Oxidation Barrier Coating, April 2011. Thesis.
[56] G. Ramírez, S.E. Rodil, S. Muhl, D. Turcio-Ortega, J.J. Olaya, M. Rivera, E. Camps, L. Escobar- Alarcón, Amorphous niobium oxide thin films, J. Non-Cryst. Solids 356 (50-51) (2010) 2714–2721.
[57] J.M. Chappé, P. Carvalho, S. Lanceros-Mendez, M.I. Vasilevskiy, F. Vaz, A.V. Machado, M. Fenker, E. Alves, Influence of air oxidation on the properties of decorative NbOxNy coatings prepared by reactive gas pulsing, Surf. Coat. Technol. 202 (11) (2008) 2363.